ADVANCED PHOTONICS RESEARCH
Open Access
www.adpr-journal.com

Tamm Plasmon-Polariton Ultraviolet Lasers

Wen-Hui Xu, Yu-Hsun Chou, Zih-Ying Yang, Yi-Yun Liu, Min-Wen Yu, Chen-Hang Huang, Chun-Tse Chang, Chen-Yu Huang, Tien-Chang Lu, Tzy-Rong Lin, and Kuo-Ping Chen**

The ZnO-based Tamm plasmon-polariton (TPP) ultraviolet laser is realized with the strong electric field confinement in the active layer. A coupling between TPPs and photons with a Rabi splitting of ≈30 meV is observed at room temperature. Furthermore, the TPP lasing at 373 nm is clearly observed by optical pumping. The corresponding lasing characteristics, such as threshold energy, linewidth, and angular dispersion curve are verified. These results form a basis for better understanding of the TPPs lasing mechanisms.

1. Introduction

Plasmonic resonance has received great attention for decades due to strong localization of electromagnetic fields. The well-known plasmon state, like surface plasmon polaritons (SPPs) and localized surface plasmon (LSP), have been intensively studied for many possible applications, such as nanoantennas,[1,2] biosensors,[3,4] metasurface,[5] hot-electron nanoscopy,[6] and energy harvesting.[7,8] In recent times, another plasmon state which behaves like an electron surface state, also known as a Tamm plasmon-polariton (TPP), has been investigated.[9] A Tamm plasmon structure is composed of a distributed Bragg reflector (DBR) and a metal film, as was first proposed by Kaliteevski et al. in 2007.[10] Unique optical phenomenon can be observed for TPPs, including a sharp resonance and strong electric field confinement at the interface between the DBR and the metal layer.[11] Unlike SPPs, TPPs can be excited directly without a coupler or prism.[12] As TPP-based structures do not require any patterning, the fabrication of TPPs device is straightforward and would be able to scale up to larger sizes. TPPs have been applied in sensors,[13,14] thermal emitters,[15,16] hot-electrons collection,[17] enhancement of light absorption,[18,19] and nanofocusing.[20] Due to the strong field confinement of TPPs, it would also be a suitable structure for investigating the effect of Rabi splitting as well as the performance of strong coupling.[21–26] Under strong coupling conditions, TPP and excitons will form a new quasi-particle-Tamm plasmon exciton–polariton. Compared with excitons, its equivalent mass is smaller, so it is easier to form Bose–Einstein condensation than excitons. When the Tamm plasmon exciton–polariton is condensed by stimulated scattering in the final state, a lower laser threshold will be achieved. Furthermore, a Tamm plasmon cavity may facilitate integration with electrical pumping, which has great potential for the development of electrical excitation devices in the future.

One of the most important applications of strong coupling would be the cavity–emitter coupling, such as photoluminescence modification and lasing under strong coupling.[27,28]

W.-H. Xu, Y.-Y. Liu, C.-Y. Huang, K.-P. Chen
Institute of Imaging and Biomedical Photonics
National Chiao Tung University and National Yang Ming Chiao Tung University
301 Gaofa 3rd Road, Tainan 71150, Taiwan
E-mail: kpchen@nycu.edu.tw

Y.-H. Chou
Department of Photonics
National Cheng Kung University
No. 1, University Road, Tainan City 701, Taiwan (ROC)

Z.-Y. Yang
Institute of Lighting and Energy Photonics
National Chiao Tung University and National Yang Ming Chiao Tung University
301 Gaofa 3rd Road, Tainan 71150, Taiwan

The ORCID identification number(s) for the author(s) of this article can be found under https://doi.org/10.1002/adpr.202100120.

DOI: 10.1002/adpr.202100120

M.-W. Yu, C.-H. Huang
College of Photonics
National Chiao Tung University and National Yang Ming Chiao Tung University
301 Gaofa 3rd Road, Tainan 71150, Taiwan

C.-T. Chang, T.-C. Lu
Department of Photonics
National Chiao Tung University and National Yang Ming Chiao Tung University
Hsinchu 300, Taiwan
E-mail: timtclu@nycu.edu.tw

T.-R. Lin
Institute of Optoelectronic Sciences
National Taiwan Ocean University
Keelung 20224, Taiwan

T.-R. Lin
Department of Mechanical and Mechatronic Engineering
National Taiwan Ocean University
Keelung 20224, Taiwan

In conventional design of semiconductor microcavity, the optical cavity between two DBRs is usually adopted because of their high reflectivity. However, the distributed reflections at multiple interfaces of DBR make the electric field of the cavity to penetrate the DBRs yielding a relatively weak optical confinement of the electric field in the semiconductor microcavity. Conventional DBR cavities would lead to only a small Rabi splitting between two polariton modes, which makes the polariton lasing under strong coupling relatively difficult. To achieve well-confined photons, one DBR is replaced by a metal mirror with a penetration depth less than 30 nm; this could improve the field confinement and form TPPs in the active layer. Comparing with conventional microcavity devices, TPP could provide stronger field confinement at the interface of metal and DBR, which allows the active layer to be thinner than the traditional cavity length and attains higher possibility to achieve strong coupling and lower threshold operation.

Several researchers used an InGaAs quantum well (QW) embedded in TPP structures for realizing TPP lasers.[29–31] However, the binding energy of InGaAs is so small that the effects of coupling are not obvious. Moreover, the device requires an epitaxial fabrication process, which is expensive and limited by the substrate choice. Therefore, the large binding-energy material, ZnO, can be a good candidate as an active layer to replace the QW. In addition, ZnO has a large bandgap, which could act as an ultraviolet (UV) lasing source. In addition, ZnO thin films could be easily fabricated by magnetron sputtering. A combination of ZnO and TPP structures would more easily achieve strong coupling and enable coherent TPP emission without population inversion, showing smaller lasing threshold than that for a traditional cavity laser.[32,33] Some researchers also investigated the phenomenon of exciton–polaritons interactions with transition metal dichalcogenide (TMDC) embedded in TPP structures.[34,35] However, less discussion is devoted to the UV wavelength region, and none covers the lasing generation. A UV laser is an emerging tool for applications such as drug detection, protein analysis, DNA sequencing, medical imaging/therapy, curing, and lithography.[36] Therefore, in this study, a TPP laser with a ZnO thin film was developed for the UV region. ZnO has a direct bandgap of 3.35 eV and a large binding energy of 60 meV.[37] These properties contribute to observe with anticrossing of strong coupling at the UV wavelength region.

In this study, we demonstrate the TPP laser at 373 nm. By tuning the incident angle from 0° to 60°, the coupling between excitons and TPPs can be observed when the angle is larger than 30°. To discuss the anticrossing and strong coupling, the coupled oscillator model was used to fit the upper polariton branch (UPB) and lower polariton branch (LPB). Finally, we investigated the lasing spectra with different pumping densities and showed that lasing occurs when the pumping density exceeds 235 Wcm^{-2} with the linewidth decreasing to 0.693 nm.

2. Fabrications

The DBR was composed of 25 layers of Ta_2O_5/SiO_2 on a Si substrate by the electron beam evaporation process. Next, a 36 nm-thick ZnO thin film was deposited on a DBR by the RF magnetron sputtering (BRANCHY TECHNOLOGY Sputter S100B). Finally, a 36 nm-thick silver layer was deposited on top of the ZnO by the electron beam evaporation. The central wavelength of the DBR was 420 nm. **Figure 1**a shows the schematic diagram of the proposed structure. In addition, the corresponding cross-sectional transmission electron microscopy (TEM) image is shown in Figure 1b.

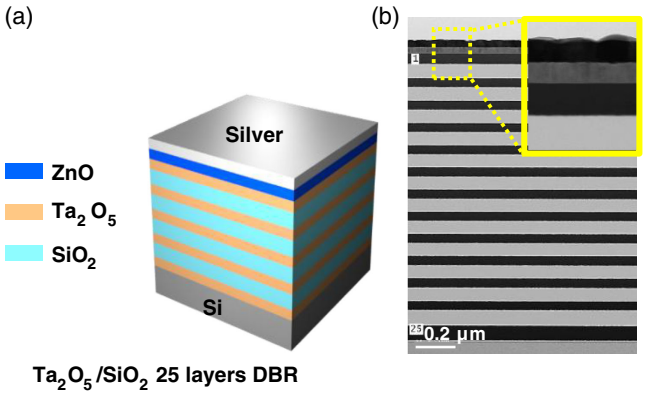

Figure 1. a) Schematic diagram of the proposed structure. The 36 nm-thick ZnO and 36 nm-thick silver layers were deposited on the top of the DBR consisting of 25 layers of Ta_2O_5 and SiO_2. b) A cross-sectional TEM image of the sample. The inset in yellow block shows high quality of the thin films. The films are silver, ZnO, Ta_2O_5, and SiO_2 from the top layer to the bottom layer.

3. Results and Discussions

Figure 2 shows the experimental results for the reflectance spectra of the DBR and TPP samples measured by UV/Vis/NIR

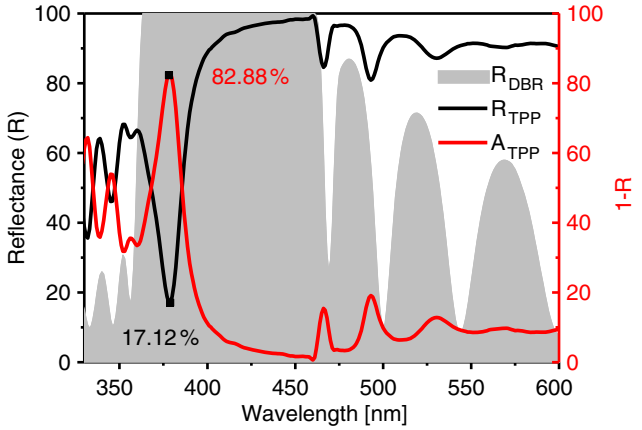

Figure 2. Measured reflectance spectra of TPP structure (black line) and bare DBR (gray area). UV–vis–NIR spectroscopy was used for the measurement. By adding the ZnO and the silver layer on the top of the DBR, the resonant dip appears within the stopband of DBR which is indicated as the black line. The red line indicates the absorptance of TPP resonance. As the substrate is a single side-polished silicon substrate, the transmission spectra are ≈0 at visible wavelength. Therefore, we defined absorption (A) as 1-R (reflectance). The red line is the absorptance spectra of the TPP structure, and the black square indicates the absorptance value at the resonance wavelength of Tamm plasmon.

spectroscopy (HITACHI U4100). These spectra are used to characterize the TPP resonance. The reflectance dip within the stopband region of the DBR can be observed at 379 nm with a value of 17.12%. The TPPs enables strong electric field confinement at the interface of the silver layer and the DBR. To enhance the coupling between excitons and TPPs, the 36 nm ZnO thin film was deposited at the interface between the silver film and the DBR. **Figure 3**a shows the electric field distribution in which the strong electric field confinement can be clearly observed at the TPP resonance wavelength. The finite element method, commercial software (COMSOL Multiphysics) was used to calculate the electric field distribution. In this modeling, we adopted 2D structures in the models where the periodic boundary conditions are used. The electric field distribution ($|E|$) was extracted along the structure. Moreover, the resonant wavelength can be adjusted by varying the thickness of the ZnO thin film. As the thickness of the ZnO film was smaller than half of the optical path length, only the Tamm plasmon mode could exist. The emission spectra of excitons of the ZnO film are investigated by photoluminescence (PL) spectroscopy (Princeton Instrument); these spectra are shown in Figure 3b. The PL peak was observed at around 383 nm.

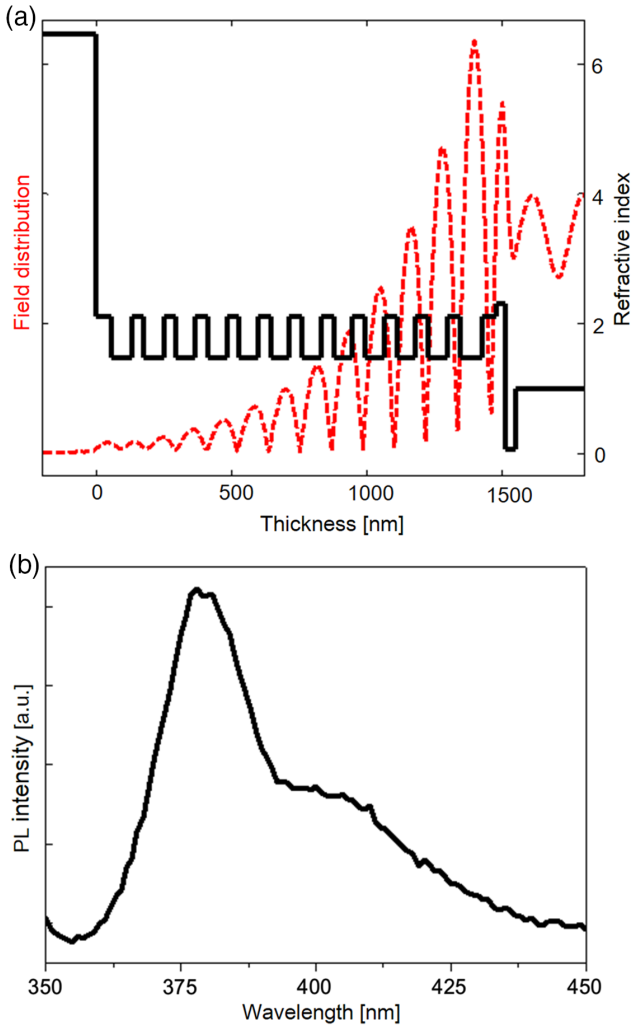

Figure 3. a) The electric field distribution at resonant wavelength = 379 nm and the refractive index profile (from left to right: Si substrate, TPP structure, and air) for the proposed TPP structure. Using Tamm plasmon structure, strong electric fields could be localized at the interface between the DBR and the metal layer. This feature can be used to confine photons in the ZnO layer. b) The optical properties of ZnO were confirmed by PL spectroscopy measurements with the excitation wavelength at 355 nm. The PL peak of ZnO was at a wavelength of ≈383 nm.

To realize the TPP laser, we investigate the reflectance spectra at room temperature to explore whether the structure has a TPP mode. As the ZnO film in this experiment is made by electron beam evaporation, the formed film is polycrystalline, which causes excitons to have strong inhomogeneous linewidth broadening and weaker oscillation strength at room temperature. At room temperature, we only consider the coupling of TPP mode and cavity mode (MC) to verify the existence of TPP mode in our structure The reflectance spectra in TE polarization were measured at different incident angles, ranging from 0° to 60°. In simulation model, the refractive index of dielectrics was obtained from ellipsometry measurements and fitted by an oscillator model. Silver is from Johnson and Christy's database.[38] Transfer matrix method was used to calculate the reflectance spectrum. The simulation and experimental results shown in **Figure 4** are in good agreement. The resonant dip becomes broader due to the coupling phenomenon when the incident angle exceeds 30°. The discrepancy between the simulation and experimental results might be due to the structural imperfection during the sample fabrication. The optical path length increases with an increase in the incident angle; thus, the influence of the imperfections could be more significant and might lead to a shallower dip in the measured reflectance spectra compared with the simulation results.

To investigate the coupling between TPPs and MC directly, the dispersion curve was fitted with the coupled oscillator model[39]

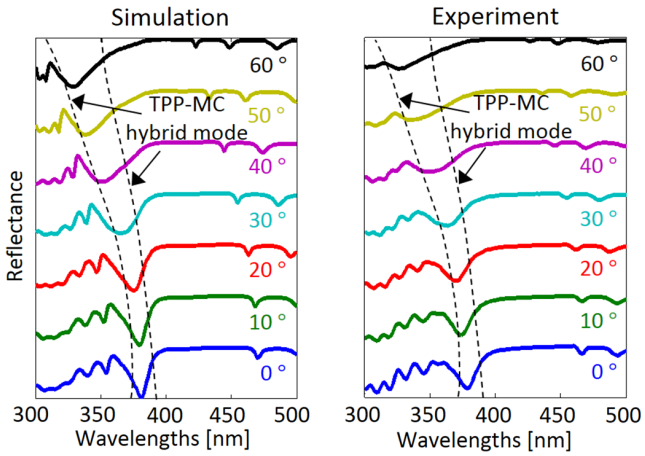

Figure 4. Reflectance spectra at different incident angles ranging from 0° to 60° with an interval of 10°. Simulation results are compared with room temperature experimental results. The resonant dip is blueshifted when the incident angle increases. The resonance shows splitting when the incident angle is larger than 30°. The dashed guiding lines show the TPP–MC hybrid modes.

$$\begin{bmatrix} E_{TPP}(\theta) - E & V \\ V & E_{MC} - E \end{bmatrix} \begin{bmatrix} \alpha \\ \beta \end{bmatrix} = 0 \quad (1)$$

where E_{MC} and E_{TPP} correspond to the energy levels of MCs and Tamm modes coupled by the interaction potential V (about 15 meV), respectively, α is the proportion of the TPPs occupied in the energy mode E, and β is the proportion of excitons occupied in the energy mode E, provided that $|\alpha|^2 + |\beta|^2 = 1$.

The dispersion curve can be given by

$$E_{+,-}(\theta) = \frac{1}{2}\left[E_{MC} + E_{TPP}(\theta) \pm \sqrt{(4V^2 + (E_{MC} - E_{TPP}(\theta))^2)}\right] \quad (2)$$

From Equation (2), two hybrid modes E_+ and E_- can be observed. The results of the modeling are shown in **Figure 5** (black dashed line) along with experimental and simulation results. The two white dashed lines represent the MC and Tamm mode, respectively.

At the emission angle of 32°, the anticrossing with splitting energy of 30 meV could be observed. The resonant dip of Tamm mode is designed to be at 379 nm because the detuning between MC and TPP affects the coupling effect.[40] When the incident angle becomes larger, the E_+ more likely represents the Tamm mode and E_- more likely represents the MC, which indicates the hybrid nature of the TPP–MC hybrid interactions between the MC and TPPs. The relatively blur dips in angle-resolved spectra are mainly due to the linewidth broadening of the Tamm mode and the MC.

To further realize UV Tamm plasmon exciton–polariton laser, we placed the sample in a cryogenic temperature environment of

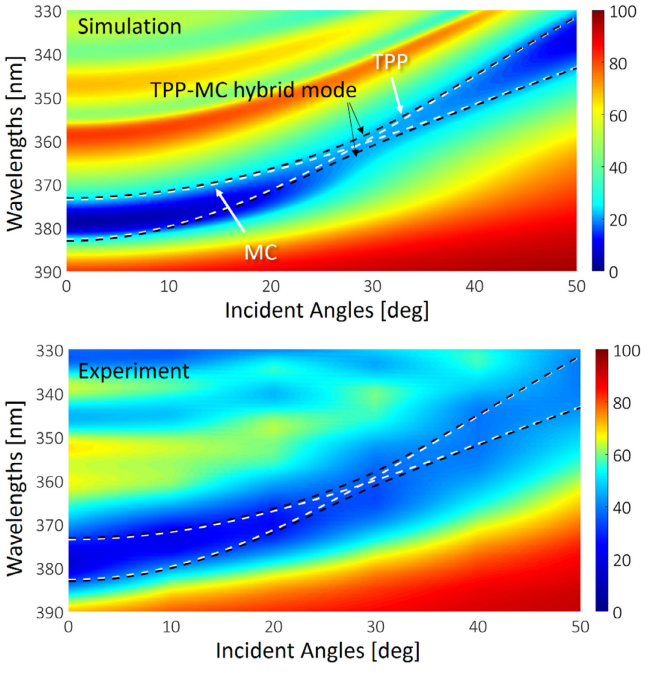

Figure 5. Angle-resolved reflectance spectra from experiment and simulation at room temperature. The black dashed lines represent two TPP–MC hybrid modes branches. The white dashed lines represent the Tamm mode and MC modes.

77 K, the 2D map of the angle-resolved photoluminescence (ARPL) spectra with the power density of 207 Wcm^{-2}, as shown in **Figure 6**a, was obtained. The sample was pumped by Nd:YVO_4 pulse lasers at 355 nm with a repetition rate and pulse duration of 1 kHz and 0.5 ns, respectively. The focused spot size was ≈15 μm in diameter. The light emitted from the sample was collected and transmitted through a UV optical fiber of the core size 600 μm. A 320 mm single monochromator attached to the nitrogen-cooled charge-coupled device (CCD) was used to analyze the emission signals from the sample. The polariton relaxation to the low k-state might be due to polariton–polariton scattering and polariton–phonon scattering (Figure 6a). The strong PL signal at 373 nm in ARPL spectra indicates this phenomenon with the LPB curve fitted with Equation (2). However, the difference between the exciton mode and the detuning from Figure 5 is due to the different measurement positions and temperature.[40]

In laser pumping experiments, the emission lasing spectra were obtained using different pumping power densities ranging from 21.6 to 324 Wcm^{-2}, as shown in Figure 6b. The continuous increase in the pumping density leads to a spontaneous emission with a threshold of ≈235 Wcm^{-2} and a linewidth decrease to 0.693 nm. In our experiment, the device was pumped by an Nd:YVO_4 pulse laser and the fluctuation of the laser power was lower than 1%. which is because the output from power supply might have some subtle fluctuations. Furthermore, under the higher pumping power densities, the multiple lasing peaks appear in the spectra. These peaks can be attributed to the transverse modes within the pumping laser spot.[41,42] Moreover, the lasing peak on the far left of Figure 6b is blueshifted in Figure 6d and the linewidth slightly increases when the pumping power densities are larger than the threshold, as shown in Figure 6c, which is due to polariton–polariton interactions. The result shows the features of polariton lasers in the TPP devices.[32,40]

4. Conclusions

We demonstrated that UV lasing generation can be achieved by ZnO-based TPP devices. The electric fields can be confined near the ZnO active layer to form a strong coupling with the Rabi splitting and small mode volume. Comparing with a conventional microcavity laser, the cavity length must be at least half the emission wavelength. In this work, the ZnO film is only 1/10 the thickness of the wavelength, and only half the thickness of the traditional microcavity structure.[43] Because the TPP mode has the ability to confine the electric field in the surface between DBR and metal, light, and matter can interact in such a small space to form polaritons. Polaritons can condensate at the ground state through stimulated scattering, forming polariton emissions. Due to the strong coupling effect, the laser emission can still be achieved in such a thin ZnO layers. The ZnO TPP laser is a cost effective, easy-to-fabricate device which has a relatively large sample area. In addition, not only the semiconductor materials but also the organic materials have been applied in UV TPP research.[44,45] The UV TPP laser can be used to further realize polariton devices such as polaritronic all-optical logic gates, the critical coupling vortex,[46] the chiral selective emitters,[47] or the tunable bound states in the continuum.[48] Moreover, the UV laser has the potential for biomedical applications such

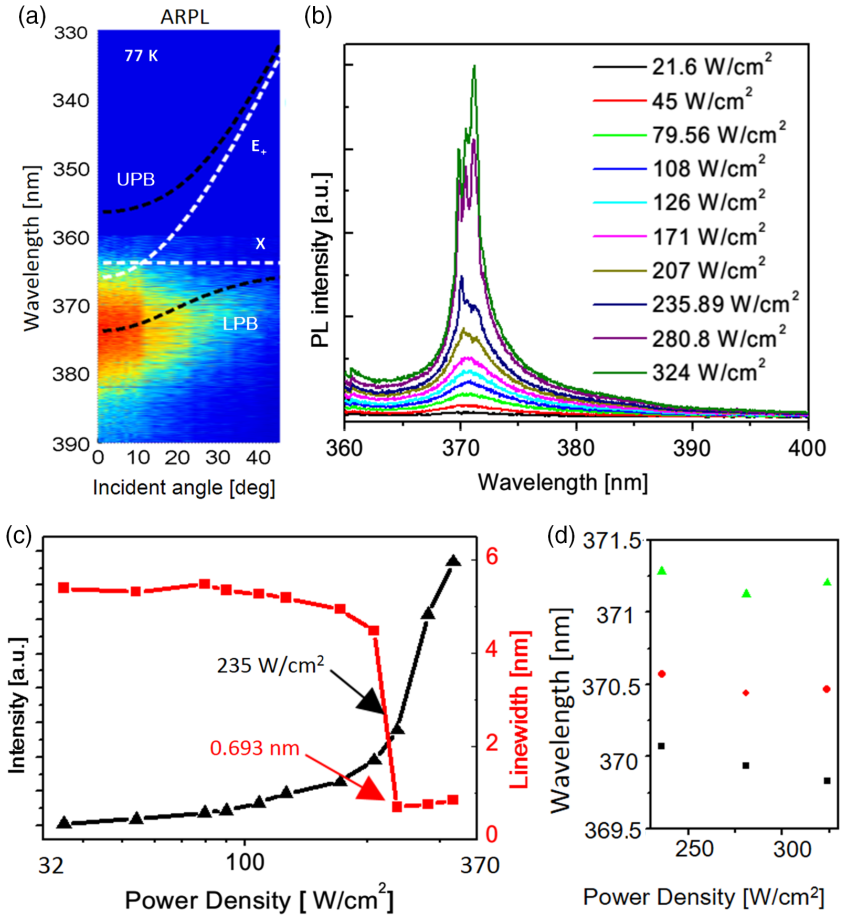

Figure 6. a) ARPL spectra excited by the lasers with the power density of 235 Wcm^{-2}. The phenomenon at lower LPB represents light emission at the ground state, which also means that the polariton relaxes to the ground state. b) Lasing spectra at different power densities. The multiple peaks can be observed clearly. c) Intensity and linewidth of the lasing peak on the far left for different power densities. In contrast with the conventional photon laser, the lasing generation increases when the pumping power density is larger than the threshold. d) Shifts of the lasing wavelengths with the pumping power density exceeding the threshold.

as eliminating cancer cells or tumors or for sensing applications in DNA or proteins.

Supporting Information

Supporting Information is available from the Wiley Online Library or from the author.

Acknowledgements

W.-H. Xu and Y.-H. Chou contributed equally to this work. This work was supported by the Higher Education Sprout Project of the National Yang Ming Chiao Tung University and Ministry of Education and the Ministry of Science and Technology (MOST 107-2221-E-009-046-MY3; 108-2923-E-009-003-MY3; 109-2628-E-009 −007-MY3; 110-2923-E-009 −005 -MY2; MOST 109-2636-M-006-014). Specially thanks for Chen Yang's assistance in AFM measurement.

Conflict of Interest

The authors declare no conflict of interest.

Data Availability Statement

The data that support the findings of this study are available from the corresponding author upon reasonable request.

Keywords

Tamm plasmon-polaritons, ultraviolet lasers, ZnO

Received: April 29, 2021
Revised: September 10, 2021
Published online: November 25, 2021

[1] A. Kinkhabwala, Z. Yu, S. Fan, Y. Avlasevich, K. Müllen, W. Moerner, *Nat. Photonics* **2009**, *3*, 654.
[2] J.-H. Yang, K.-P. Chen, *Sci. Rep.* **2016**, *6*, 32194.
[3] K. M. Mayer, J. H. Hafner, *Chem. Rev.* **2011**, *111*, 3828.
[4] M. L. Coluccio, F. Gentile, G. Das, A. Nicastri, A. M. Perri, P. Candeloro, G. Perozziello, R. P. Zaccaria, J. S. T. Gongora, S. Alrasheed, *Sci. Adv.* **2015**, *1*, e1500487.

[5] A. V. Kildishev, A. Boltasseva, V. M. Shalaev, *Science* **2013**, *339*, 1232009.
[6] A. Giugni, B. Torre, A. Toma, M. Francardi, M. Malerba, A. Alabastri, R. P. Zaccaria, M. I. Stockman, E. Di Fabrizio, *Nat. Nanotechnol.* **2013**, *8*, 845.
[7] H. A. Atwater, A. Polman, *Nat. Mater.* **2010**, *9*, 205.
[8] M.-Y. Lu, C.-Y. Tsai, H.-A. Chen, Y.-T. Liang, K.-P. Chen, S. Gradečak, S. Gwo, L.-J. Chen, *Nano Energy* **2016**, *20*, 264.
[9] M. Sasin, R. Seisyan, M. Kalitteevski, S. Brand, R. Abram, J. Chamberlain, A. Y. Egorov, A. Vasilev, V. Mikhrin, A. Kavokin, *Appl. Phys. Lett.* **2008**, *92*, 251112.
[10] M. Kaliteevski, I. Iorsh, S. Brand, R. Abram, J. Chamberlain, A. Kavokin, I. Shelykh, *Phys. Rev. B* **2007**, *76*, 165415.
[11] B. J. Lee, Z. Zhang, *J. Heat Transfer* **2007**, *129*, 17.
[12] C.-Y. Chang, Y.-H. Chen, Y.-L. Tsai, H.-C. Kuo, K.-P. Chen, *IEEE J. Sel. Top. Quantum Electron.* **2015**, *21*, 262.
[13] B. Auguié, M. C. Fuertes, P. C. Angelomé, N. L. Abdala, G. J. Soler Illia, A. Fainstein, *ACS Photonics* **2014**, *1*, 775.
[14] S.-G. Huang, K.-P. Chen, S.-C. Jeng, *Opt. Mater. Express* **2017**, *7*, 1267.
[15] Z.-Y. Yang, S. Ishii, T. Yokoyama, T. D. Dao, M.-G. Sun, P. S. Pankin, I. V. Timofeev, T. Nagao, K.-P. Chen, *ACS Photonics* **2017**, *4*, 2212.
[16] Z.-Y. Yang, S. Ishii, T. Yokoyama, T. D. Dao, M.-G. Sun, T. Nagao, K.-P. Chen, *Opt. Lett.* **2016**, *41*, 4453.
[17] C. Zhang, K. Wu, V. Giannini, X. Li, *ACS nano* **2017**, *11*, 1719.
[18] H. Lu, X. Gan, D. Mao, Y. Fan, D. Yang, J. Zhao, *Opt. Express* **2017**, *25*, 21630.
[19] H. Lu, Y. Li, Z. Yue, D. Mao, J. Zhao, *APL Photonics* **2019**, *4*, 040801.
[20] L. Niu, Y. Xiang, W. Luo, W. Cai, J. Qi, X. Zhang, J. Xu, *Sci. Rep.* **2016**, *6*, 39125.
[21] Z. Wang, R. Gogna, H. Deng, *Appl. Phys. Lett.* **2017**, *111*, 061102.
[22] P. Forn-Díaz, L. Lamata, E. Rico, J. Kono, E. Solano, *Rev. Mod. Phys.* **2019**, *91*, 025005.
[23] A. F. Kockum, A. Miranowicz, S. De Liberato, S. Savasta, F. Nori, *Nat. Rev. Phys.* **2019**, *1*, 19.
[24] D. Polak, R. Jayaprakash, T. P. Lyons, L. Á. Martínez-Martínez, A. Leventis, K. J. Fallon, H. Coulthard, D. G. Bossanyi, K. Georgiou, A. J. Petty, J. Anthony, *Chem. Sci.* **2020**, *11*, 343.
[25] F. Ge, X. Han, J. Xu, *Laser Photonics Rev.* **2021**, *15*, 2000514.
[26] F. J. Garcia-Vidal, C. Ciuti, T. W. Ebbesen, *Science* **2021**, *373*, 6551.
[27] P. Bhattacharya, B. Xiao, A. Das, S. Bhowmick, J. Heo, *Phys. Rev. Lett.* **2013**, *110*, 206403.
[28] P. Bhattacharya, T. Frost, S. Deshpande, M. Z. Baten, A. Hazari, A. Das, *Phys. Rev. Lett.* **2014**, *112*, 236802.
[29] C. Symonds, G. Lheureux, J.-P. Hugonin, J.-J. Greffet, J. Laverdant, G. Brucoli, A. Lemaitre, P. Senellart, J. Bellessa, *Nano Lett.* **2013**, *13*, 3179.
[30] G. Lheureux, S. Azzini, C. Symonds, P. Senellart, A. Lemaître, C. Sauvan, J.-P. Hugonin, J.-J. Greffet, J. Bellessa, *ACS Photonics* **2015**, *2*, 842.
[31] C. Symonds, A. Lemaître, P. Senellart, M. Jomaa, S. Aberra Guebrou, E. Homeyer, G. Brucoli, J. Bellessa, *Appl. Phys. Lett.* **2012**, *100*, 121122.
[32] D. Bajoni, *J. Phys. D: Appl. Phys.* **2012**, *45*, 313001.
[33] A. Imamog, R. Ram, S. Pau, Y. Yamamoto, *Phys. Rev. A* **1996**, *53*, 4250.
[34] N. Lundt, S. Klembt, E. Cherotchenko, S. Betzold, O. Iff, A. V. Nalitov, M. Klaas, C. P. Dietrich, A. V. Kavokin, S. Höfling, *Nat. Commun.* **2016**, *7*, 13328.
[35] T. Hu, Y. Wang, L. Wu, L. Zhang, Y. Shan, J. Lu, J. Wang, S. Luo, Z. Zhang, L. Liao, *Appl. Phys. Lett.* **2017**, *110*, 051101.
[36] P. Dumon, W. Bogaerts, V. Wiaux, J. Wouters, S. Beckx, J. Van Campenhout, D. Taillaert, B. Luyssaert, P. Bienstman, D. Van Thourhout, *IEEE Photonics Tech. Lett.* **2004**, *16*, 1328.
[37] Ü. Özgür, Y. I. Alivov, C. Liu, A. Teke, M. Reshchikov, S. Doğan, V. Avrutin, S.-J. Cho, H. Morkoc, *J. Appl. Phys.* **2005**, *98*, 11.
[38] P. B. Johnson, R.-W. Christy, *Phys. Rev. B* **1972**, *6*, 4370.
[39] X. Liu, T. Galfsky, Z. Sun, F. Xia, E.-C. Lin, Y.-H. Lee, S. Kéna-Cohen, V. M. Menon, *Nat. Photonics* **2015**, *9*, 30.
[40] Y.-Y. Lai, Y.-P. Lan, T.-C. Lu, *Light Sci. Appl.* **2013**, *2*, e76.
[41] Y.-Y. Lai, Y.-H. Chou, Y.-S. Wu, Y.-P. Lan, T.-C. Lu, S.-C. Wang, *Appl. Phys. Express* **2014**, *7*, 062101.
[42] Y.-H. Chou, B.-T. Chou, C.-K. Chiang, Y.-Y. Lai, C.-T. Yang, H. Li, T.-R. Lin, C.-C. Lin, H.-C. Kuo, S.-C. Wang, *ACS Nano* **2015**, *9*, 3978.
[43] Z.-Y. Yang, S. Ishii, A. T. Doan, S. L. Shinde, T. D. Dao, Y.-P. Lo, K.-P. Chen, T. Nagao, *Adv. Opt. Mater.* **2020**, *8*, 1900982.
[44] K. M. Morozov, K. A. Ivanov, A. V. Belonovski, E. I. Girshova, D. D. S. Pereira, C. Menelaou, P. Pander, L. G. Franca, A. P. Monkman, G. Pozina, *J. Phys. Chem. C* **2020**, *124*, 21656.
[45] B. Liu, R. Wu, V. M. Menon, *J. Phys. Chem. C* **2019**, *123*, 26509.
[46] R. G. Bikbaev, D. N. Maksimov, P. S. Pankin, K.-P. Chen, I. V. Timofeev, *Opt. Express* **2021**, *29*, 4672.
[47] M.-Y. Lin, W.-H. Xu, R. G. Bikbaev, J.-H. Yang, C.-R. Li, I. V. Timofeev, W. Lee, K.-P. Chen, *Materials* **2021**, *14*, 2788.
[48] B.-R. Wu, J.-H. Yang, P. S. Pankin, C.-H. Huang, W. Lee, D. N. Maksimov, I. V. Timofeev, K.-P. Chen, *Laser Photonics Rev.* **2021**, *15*, 2000290.